A Theory for El Nino Cycle

WANG Bin
Department of Meteorology
School of Ocean and Earth Science and Technology
University of Hawaii at Manoa
2525 Correa Road
Honolulu, HI 96822, U. S. A.

Abstract

A theoretical model for the coupled tropical ocean and atmosphere is derived from physical principles. The model characterizes the temporal evolution of the El Nino cycle as a second order nonlinear dynamic system. With an annual mean basic state the model has, for a rather restricted range of air-sea coupling strength, a unique limit cycle solution which is a stable attractor representing a regular interannual oscillation of the coupled ocean and atmosphere. The oscillation is characterized by a delicate phase lead of thermocline displacement to SST, which agrees well with observations. This phase lead results from a nonlinear interaction between SST and thermocline variations and plays a critical role in providing a negative feedback to turn a warming to a cooling or vice versa, sustaining the oscillation.

When the basic state varies annually, the limit cycle develops a strange attractor and the interannual oscillations exhibit deterministic chaos. We show that the basic state is most unstable (stable) in northern spring (fall). The season-dependent development of the coupled mode causes a phase "lock" of the ENSO cycle with annual cycle—the transition phases of the oscillation tend to occur during most unstable season—which, in turn, causes the irregularities in the oscillation period and amplitude.

I. Introduction

1. *Observed features of the El Nino cycle*

The spatial structure of the Pacific warming (El Nino) is characterized by a positive SST anomaly trapped in the eastern-central basin, nearly meridionally symmetric relative to the equator. As visualized by Bjerknes (1966, 1969), the warming is closely associated with westerly anomalies over the equatorial western and central Pacific. The latter is a manifest of the pressure rising over Asian-Australian monsoon region and a drop over the trade winds region (the Southern Oscillation).

The temporal structure of the El Nino cycle or Southern Oscillation exhibits the following characteristic features: (1) quasi-periodicity with a period ranging from two to seven years; (2) prominent irregularities in the amplitude and period of the oscillation (Gu and Philander, 1995; Wang, B., and Y. Wang, 1995); (3) seasonal dependence of the evolution: warming tends to start in the warm season of the annual cycle and matures in the central Pacific toward the end of a calendar year (Rasmusson and Carpenter, 1982).

2. *Background in theoretical studies*

In the last decades or so, a large number of theoretical studies have been carried out to

explain fundamental mechanisms of El Nino-Southern Oscillation (ENSO). They deal with primarily two issues: (Ⅰ) What causes the initial grow of the SST and wind anomalies? (Ⅱ) How does the turnabout from a cold to a warm state take place?

The question Ⅰ was first addressed conceptually by Bjerknes (1969). He attributed the cause of the warming to a positive feedback between the atmospheric Walker circulation and the oceanic thermal contrast between the western Pacific warm pool and eastern Pacific cold tongue. This hypothesis has greatly inspired succeeding theoretical studies of the properties of the coupled ocean and atmosphere system. Philander et al. (1984) presented first rigorous stability analysis of a coupled shallow water system on equatorial beta-plane. Additional mechanisms and extensions were made by many ensuing studies (see review of McCreary and Anderson, 1991; Neelin et al., 1994). The development of a warm episode is now understood as resulting from the coupled instability of a mean state of the atmosphere and ocean.

The question Ⅱ was a Bjerknes' (1969) puzzle. It is much more difficult for simple theoretical models to address because of the complexity and nonlinearity of the coupled ocean-atmosphere system. Consequently, numerical modeling of ENSO became a popular approach. Among them, the intermediate coupled models are theoretician's favorable tools for understanding physics of the coupled system. Zebiak and Cane (1987) first aspired to address Bjerknes' puzzle by examining the cause of the oscillation in their model and found that the equatorial heat content increases prior to warm events and decreases sharply during the events. The variability in the heat content of the upper ocean was identified as a critical element of the model oscillation.

Primarily based upon the understanding gained from numerical experiments with intermediate models, Saurez and Schopf (1988) and Battisti and Hirst (1989) put forward a semi-empirical analogue model for ENSO—the delayed oscillator model. Their models interpret the turn over from a warming to cooling as resulting from the reflected equatorial waves at the western boundary which provide a delayed, negative feedback to "shot down" the original growth in the eastern Pacific. The delay which plays a central role in the above argument results from ocean wave dynamics as shown by Cane et al. (1990) and Schopf and Saurez (1990).

The delayed-oscillator model shows certain degree of consistence with observed thermocline variability (Kessler, 1990) and the occurrence of large-scale baroclinic waves traversing the ocean basin in some coupled GCMs (e.g., Latif et al., 1993). However, the reflection of Rossby waves at the western boundary prior to the onset of an El Nino has not been clearly identified by observations. The model that removes western boundary reflection remains to be capable of simulating ENSO-like variation (Wang and Wesburg, 1994). In addition, the analogue models are not rigorously derived from physical principles and they do not explain the irregularity and season-dependence of ENSO.

3. *Theoretical targets*

Our theory is aimed at addressing the following fundamental questions:

•Why does the climate of the coupled tropical ocean-atmosphere system oscillate? What determines its predominant period and amplitude?

•Why is the oscillation so irregular? Is it an inherent behavior of the nonlinear coupled climate system?

•Why does the warming often start in the warm season of the year? Why does the persistence of the Southern Oscillation break down in boreal spring?

We will derive a theoretical model from the first principles with the aid of a number of simplifications. To facilitate analysis, we keep the model as simple as possible. Hence only most relevant physics are included. The characteristic spatial structure of the El Nino anomalies allows for a crucial reduction of the three-dimensional model to one-dimensional that focuses on the eastern equatorial Pacific Nino-3 region (5°N—5°S, 150°-90°W). The one-dimensional model—a nonlinear dynamicsystem—is capable of reproducing irregular interannual oscillation that considerably resembles ENSO. The model is therefore instrumental for understanding the mechanisms of the irregular oscillation and the seasonal dependence of ENSO.

I. Theoretical model for the coupled tropical ocean-atmosphere

The trapping of ENSO warming in the eastern equatorial Pacific manifests the importance of climatological mean states. To delineate relevant physics of ENSO, it is wise to treat ENSO as a low-frequency departure from its climatological mean (annual cycle).

Consider an active upper ocean with a mean depth of H overlays an inert deep ocean with thermocline as an interface. To better describe SST variation, the upper ocean is further divided into a well-mixed, frictional surface layer of constant-depth (H_1) (hereafter refer to as mixed-layer) and a subsurface layer (Cane, 1979).

The dominant contributor to SST variation in the equatorial eastern Pacific is the upwelling process. We will neglect horizontal advection of temperature, although inclusion of it is straight forward. The mixed-layer temperature (hereafter referred to as SST) anomaly is therefore governed by

$$\frac{\partial T}{\partial t} + \frac{w}{H_1}[T - \overline{T}_* + T - T_*(h)] + \frac{\overline{w}}{H_1}(T - T_*(h)) = -\alpha_* T, \qquad (1)$$

where overbars denote basic-state quantities; w represents upwelling at the mixed-layer base; α_* is a coefficient of Newtonian cooling that represents all processes which bring SST towards its climatology; T_* denotes temperature of subsurface water that is upwelled into the mixed-layer. In (1), we have assumed that an anomalous downwelling (or upwelling) could suppress (or enhance) mean upwelling and induce anomalous warming (or cooling). This is reasonable in the equatorial eastern Pacific where upwelling prevails nearly all the time. Further assume that all isotherms beneath the mixed-layer move in harmony with vertical thermocline displacement. A rise (deepening) of thermocline results a decrease (increase) of T_*. A simple parameterization of T_* in terms of thermocline anomaly h follows (Battisti and Hirst, 1989):

$$T_s(h) = \mu_s(\bar{h})h, \tag{2}$$

where the coefficient μ_s measures the degree of influence of thermocline fluctuation on SST.

The upwelling w is generated by two processes: the Ekman divergence in the mixed layer and the vertical displacement of the thermocline. We will consider the former being dominant and neglect the latter, although inclusion of the second contributor is not difficult. The problem becomes how to determine Ekman flow divergence. Assume that the Ekman flow V_e vanishes at the mixed layer base, thus it also represents the vertical shear between the mixed-layer and the subsurface layer. It is thus governed by (Zebiak and Cane, 1987)

$$r_1 u_e - \beta y v_e = \frac{H}{H_1} r u_s, \tag{3}$$

$$r_1 v_e + \beta y u_e = \frac{H}{H_1} r v_s, \tag{4}$$

where u_s and v_s denote zonal and meridional surface wind speed, respectively. we have linearized the bulk formula for wind stress, thus the coefficient

$$r = lU_s, \text{ and } l \equiv \frac{\rho_a}{\rho_o}\frac{C_D}{H}, \tag{5}$$

where U_s is a characteristic scale for surface wind speed; ρ_a and ρ_o the densities of the surface air and sea water, respectively; and C_D the drag coefficient.

From (3) and (4), one can solve for Ekman flow and compute its divergence so that the upwelling at the mixed-layer base w can be obtained. It can be shown that near the equator

$$w = \frac{H_1 H_2}{H}\nabla \cdot V_e \approx -H_2 \frac{r\beta}{r_1^2} u_s, \tag{6}$$

where $H_2 = H - H_1$. Equation (6) implies that an equatorial anomalous westerly induces anomalous convergence and downwelling.

The upper ocean dynamics, i. e., the thermocline anomaly h and anomalous vertical mean currents above the thermocline, u and v, can be described by a linear, reduced-gravity model on the equatorial β- plane. Here semi-geostrophic motion (long wave approximation) is assumed because the square ratio of the meridional to zonal length scale, $(L_y^2/L_x^2)^2$, is small. The anomalous meridional wind stress will be omitted because of its smallness and the dullness of the ocean to its variation. The governing equations for the entire upper ocean may then be written

$$\frac{\partial h}{\partial t} + H\left(\frac{\partial u}{\partial x} + \frac{\partial v}{\partial y}\right) = 0, \tag{7}$$

$$\frac{\partial u}{\partial t} - \beta y v = -g'\frac{\partial h}{\partial x} + r u_s, \tag{8}$$

$$\beta y u = -g'\frac{\partial h}{\partial y}. \tag{9}$$

A thermocline-depth anomaly equation can be derived from combining Equations (7)—(9):

$$y^2\frac{\partial h}{\partial t} + \frac{g'H}{\beta^2}\frac{\partial}{\partial t}\left(\frac{2}{y}\frac{\partial h}{\partial y} - \frac{\partial^2 h}{\partial y^2}\right) - \frac{g'H}{\beta}\frac{\partial h}{\partial x} = \frac{rH}{\beta}\left(y\frac{\partial u_s}{\partial y} - u_s\right). \tag{10}$$

Equation (10) describes the upper active ocean dynamics forced by zonal wind stress and

associated curl.

In the absence of the wind forcing, Equation (10) yields a free equatorial Kelvin wave and a family of free long Rossby waves. These wave solutions may be expressed in terms of generalized Laguerre functions (Appendix) which can be transformed to parabolic cylindrical functions used by Gill (1980) or Hermit polynomials used by Matsuno (1966).

With the aid of (2) and (6), the SST anomaly equation is

$$\frac{\partial T}{\partial t} = \frac{H_2 r \beta}{H_1 r_s^2} u_e (\overline{T} - \overline{T}_s + T - \mu_s h)) - \frac{\overline{w}}{H_1}(T - \mu_s h) - \alpha_s T. \tag{11}$$

Once wind stress is known, SST and h can be determined by Equations (10) and (11).

Surface winds are forced by SST gradients. A simplified Lindzen-Nigam (1987) model is used in which boundary layer winds are taken to be nondivergent so that the feedback of the free atmosphere to the boundary layer flow is negligible. This assumption is acceptable because the rotational zonal wind dominates over its divergent counterpart even in the deep tropics (Murakami and Wang, 1992). Note that the distortion of zonal winds arising from the above assumption is small over the equatorial wave guide where the ocean cares. With this simplification, the surface winds are simply given by (Wang and Li, 1993)

$$r_e u_e - \beta y v_e = dR \frac{\partial T}{\partial x}, \tag{12}$$

$$r_e v_e + \beta y u_e = dR \frac{\partial T}{\partial y}, \tag{13}$$

where r_e expresses Rayleigh frictional coefficient, d a non-dimensional depth of the atmospheric boundary layer, and R the gas constant. From Equations (12) and (13) surface wind can be solved as a function of SST. The zonal wind and the forcing in the r. h. s. of Equation (10) are

$$u_e = \frac{dR}{r_e^2 + \beta^2 y^2}\left(r_e \frac{\partial T}{\partial x} + \beta y \frac{\partial T}{\partial y}\right), \tag{14}$$

$$\left(y \frac{\partial u_e}{\partial y} - u_e\right) = \frac{-dRr_e}{r_e^2 + \beta^2 y^2} \frac{\partial T}{\partial x} + f_1(T, y), \tag{15}$$

where $f_1(T, 0) \equiv 0$. Therefore, near the equator the principal parts of wind forcing (14) and (15) are simply proportional to zonal SST gradient.

The coupled tropical ocean and atmosphere is thus governed by two prognostic equations: one for thermocline depth anomalies, Equation (10), and the other for SST, Equation (11). Equations (14) and (15) consist of a closed system with the diagnostic relations for zonal wind. The essence of this theoretical model is the nonlinear coupling between mixed-layer thermodynamics and upper-ocean dynamics through wind stress and upwelling.

Ⅱ. ENSO dynamic system

1. *Scale analysis*

The present model involves a number of basic parameters which are listed in Table 1. Based on observations, we take one-half basin width and H_1 as, respectively, the characteristic scale for zonal distance and vertical thermocline displacement.

Table 1 List of the model parameters.

Geometric parameters		
L	Zonal width of the Ocean basin	1.7×10^{7} m
H	Mean depth of the thermocline	150 m
H_1	Depth of the mixed-layer	50 m
d	Nondimensional atmospheric boundary layer depth	0.2
Geophysical Parameters		
β	Equatorial planetary vorticity gradient	2.28×10^{-11} m^{-1} s^{-1}
g'	Reduced gravity	2.8×10^{-2} m s^{-1}
$l=\rho_a C_D/\rho_0 H$	Wind stress coefficient	10^{-8} m^{-1}
Friction/damping parameters		
α_s	Newtonian cooling coefficient for SST anomaly	(125 d)$^{-1}$
r_s	Rayleigh friction coefficient in the oceanic mixed layer	(1.5 d)$^{-1}$
r_a	Rayleigh friction coefficient in atmospheric boundary layer	3.6×10^{-6} m^{-1}
Other inherent parameters		
C_0	Oceanic Kelvin wave speed	2.0 m s^{-1}
L_0	Oceanic Rossby radius of deformation	300 km
$L_z=r_s/\beta$	Ekman spreading length scale	338 km

The characteristic scale for surface zonal wind speed, U_a, can be deduced from a primary balance between wind stress and the pressure gradient force associated with the thermocline slope—the equatorial Sverdrup balance (Sverdrup, 1947) (Equation (7)). Thus,

$$U_a=\left(\frac{g'H_1}{lL_x}\right)^{\frac{1}{2}}. \tag{16}$$

From (6), the characteristic scale for anomalous upwelling

$$W=\frac{\beta g'H_1H_2}{r_s^2L_x}. \tag{17}$$

The characteristic anomalous SST scale may be determined from the equatorial zonal momentum balance in the atmospheric boundary layer (Equation (12)) which leads to

$$\theta=\frac{r_a}{dR}\left(\frac{L_xg'H_1}{l}\right)^{\frac{1}{2}}. \tag{18}$$

The local change of SST primarily results from cooling (warming) associated with the anomalous upwelling (downwelling), the time scale for SST variation is H_1/W, which yields

$$\tau = \frac{r_s^2 L_x}{\beta g' (H - H_1)}. \tag{19}$$

Generally speaking, the characteristic meridional length scale for the coupled mode, L_y, should be neither the oceanic, nor the atmospheric Rossby radius of deformation. Without loss of generality, we assume that

$$L_y = \lambda L_o, \tag{20}$$

where $L_o = \sqrt{\frac{C_0}{\beta}}$ is oceanic Rossby radius of deformation. Note that L_y is related to characteristic zonal currents scale U_0 as implied by (9). The zonal currents may be scaled by

$$U_0 = \alpha U_a, \tag{21}$$

where α is an empirical air-sea coupling coefficient that measures the ocean currents response to unit wind speed. With the aid of (21) we can show that

$$\lambda = \alpha^{\frac{1}{2}} \left(\frac{H_1}{H} L_x\right)^{\frac{1}{4}}. \tag{22}$$

Equations (20) and (22) indicate that the meridional scale of the coupled mode depends on the air-sea coupling coefficient.

Using parameter values listed in Table 1, we have $U_a = 4\ \mathrm{m\ s^{-1}}$, $W = 0.55\ \mathrm{m\ d^{-1}}$, $\theta = 2.1℃$, $\tau = 3.05$ months. These characteristic scales agree well with observations.

Using L_x, L_y, τ, θ, and H_1 to scale x, y, t, T, and h, respectively, one may obtain the following nondimensional SST and thermocline-depth equations:

$$\frac{\partial T'}{\partial t'} = \frac{\partial T'}{\partial x'}(\Delta T_0' + T' - \mu' h') + \overline{T}'_x (T' - \mu' h') - \alpha' T', \tag{23}$$

$$\delta \frac{\partial}{\partial t}\left[y'^2 h' + \varepsilon\left(\frac{2}{y'}\frac{\partial h'}{\partial y'} - \frac{\partial^2 h'}{\partial y'^2}\right)\right] - \frac{\partial h'}{\partial x'} = -\frac{\partial T}{\partial x}, \tag{24}$$

where $'$ denotes nondimensional quantities. The nondimensional basic state parameters are

$$\Delta T'_0 = (\overline{T} - \overline{T}_e)/\theta, \tag{25}$$

$$\overline{T}'_x = \frac{L_x}{\theta}\frac{\partial \overline{T}}{\partial x}, \tag{26}$$

where $\overline{T}'_x$ symbolizes zonal SST gradient or the strength of the mean upwelling. The model contains the following nondimensional numbers

$$\varepsilon \equiv \frac{g' H}{\beta^2 L_y^4} = \left(\frac{L_0}{L_y}\right)^4, \tag{27}$$

$$\delta \equiv \frac{H_2}{H}\frac{\beta^2 L_y^2}{r_s^2} = \frac{H_2}{H}\left(\frac{L_y}{L_{r_s}}\right)^2, \tag{28}$$

where $L_{r_s} = r_s/\beta$ depicts a meridional distance over which Ekman transport spreads out SST anomalies on ENSO development time scale. The nondimensional number δ measures the relative magnitude of the thermocline variation and non-Sverdrup balance. The parameter ε measures the relative importance of the wave motion to slow non-Sverdrup flow forced by

wind stress. A vanishing ϵ implies the absence of oceanic wave motion. Both δ and ϵ depend on coupled meridional scale L_y or the air-sea coupling coefficient α. Another nondimensional coupling coefficient

$$\mu' = \frac{\mu_s H_1}{\theta}. \tag{29}$$

measures the degree of influence of wind-induced thermocline fluctuation on subsurface water temperature. For convenience it will be referred to as thermocline-SST coupling coefficient.

2. *ENSO dynamic system*

The observed SST and h anomalies exhibits a spatial pattern that is nearly symmetrical and trapped to the equator. The meridional structure of the ENSO mode can, therefore, be represented roughly by the lowest-order parabolic cylindrical function

$$D_0(y') = e^{-\frac{y'^2}{4}}. \tag{30}$$

Further assume that the mean state is invariant in meridional direction. The anomalous SST and h can be written approximately as the following highly truncated form

$$T' = \tilde{T}(x', t')D_0(y'), \tag{31}$$

$$h' = \tilde{h}(x', t')D_0(y'). \tag{32}$$

Substituting (31) and (32) into Equations (23) and (24) and projecting the resultant equations onto $D_0(y')$ yield

$$\frac{\partial \tilde{T}}{\partial t'} = \Delta T_0' \frac{\partial \tilde{T}}{\partial x'} + (T_x' - \alpha')\tilde{T} - \mu' T_x' \tilde{h} + \sqrt{\frac{2}{3}} \frac{\partial \tilde{T}}{\partial x'}[\tilde{T} - \mu' \tilde{h}], \tag{33}$$

$$\frac{\partial \tilde{h}}{\partial t'} = b\left(\frac{\partial \tilde{h}}{\partial x'} - \frac{\partial \tilde{T}}{\partial x'}\right), \tag{34}$$

where

$$b \equiv \frac{2}{\delta(1 - 3\epsilon)}. \tag{35}$$

The simplest spatial finite difference form of (33) and (34) may be obtained by considering two boxes, one centered at x_E (120°W, for example) and the other at x_W (160°E, for instance), representing the eastern and western Pacific, respectively. The distance between the two boxes is taken as L_x. In consistence with observations, we further neglect SST fluctuation at the western Pacific and take thermocline fluctuation at x_W precisely 180° out of phase with that at x_E. Equations (33) and (34) then become

$$\frac{dT_E}{dt} = a_1 T_E - a_2 h_E + \sqrt{\frac{2}{3}} T_E(T_E - \mu h_E), \tag{36}$$

$$\frac{dh_E}{dt} = b(2h_E - T_E), \tag{37}$$

where T_E and h_E denote, respectively, anomalous model SST and thermocline depth averaged over the equatorial eastern Pacific (approximately the Nino-3 region). The coefficients in (36) and (37) are

$$a_1 = (\Delta T_0' + T_x' - \alpha')\big|_{x_E}, \tag{38}$$

$$a_2 = \mu T_x' \big|_{x_E}, \tag{39}$$

$$\mu = \mu' \big|_{x_E}. \tag{40}$$

The ENSO mode at the equatorial eastern Pacific is thus governed by a nonlinear dynamic system that is second order in time and differs from delayed oscillator model. The system describes the behavior of ENSO mode in the core region of El Nino (SST and thermocline variations in Nino-3 region and wind anomaly over the central Pacific); much of the fundamental features of ENSO can be modeled by this simple dynamic system.

Ⅳ. Stability of the climatological mean state and linear behavior

Equations (36) and (37) possess two steady solutions:

$$T_E^{(1)} = h_E^{(1)} = 0, \tag{41}$$

$$T_E^{(2)} = 2h_E^{(2)} = \frac{2a_1 - a_2}{\sqrt{\frac{2}{3}}(2 - \mu)}. \tag{42}$$

The first steady solution represents a climatological mean equilibrium state or an ENSO transitional phase in which both SST and h are normal. In SST-h phase space it is located at the origin and can be either a stable or an unstable focus point. Physically, the climatological equilibrium state becomes unstablewhen $a_1 + 2b > 0$ (the primary bifurcation). The corresponding growth rate of a perturbation is

$$\gamma = \frac{1}{2}(\Delta T'_0 + T'_x - \alpha'_s)\Big|_{x_E} + \frac{2}{\delta(1 - 3\varepsilon)}. \tag{43}$$

Equation (43) shows the dependence of the growth rate on the equilibrium state and the coupling coefficient α. Note that the initial growth does not depend on the coupling coefficient μ. Given the annual mean state, $T_E - T_W = -3.5℃$, $(T - T_s)\big|_{x_E} = 3℃$, the growth rate increases exponentially with increasing coupling coefficient α or decreasing meridional scale of the coupled mode (dark solid curve in Figure 1a). For given α, the growth rate varies with seasons. The strongest (weakest) growth occurs for a boreal spring (fall) mean state (Figure 1a). This is due to the weakest east-west contrast and equatorial upwelling in boreal spring favor for unstable growth.

Perturbations in the vicinity of the equilibrium state may approach (or depart from) the equilibrium state either asymptotically or oscillatorilly. The presence of an oscillatory solution (growing or damping oscillation) requires that

$$0 < \frac{a_1 - a_2}{2} - \frac{1}{2}\sqrt{a_2^2 - 2a_1a_2} < b < \frac{a_1 - a_2}{2} + \frac{1}{2}\sqrt{a_2^2 - 2a_1a_2}, \tag{44}$$

and $a_2 - 2a_1 < 0$ or

$$\mu > \frac{2}{T_x'}(\Delta T_0' + T_x' - \alpha_s'), \tag{45}$$

Equation (44) implies that the oscillatory behavior occurs only when b, therefore α takes values in a restrictive positive interval. Equation (45) means that the oscillation requires μ

exceed a critical value. Numerical results shown in Figure 1b confirm the inferences. Furthermore, the oscillation period shortens with increasing μ. The dependence of the period on α is more subtle: there exists an intermediate air-sea coupling strength (or meridional scale) for which the period is the longest for given μ (Figure 1b). The strong dependence of the oscillation period on μ hints the importance of thermocline fluctuation. The linear oscillation period also depends on basic state. For instance, as vertical temperature gradient decreases, oscillation requires considerably larger μ; meanwhile, the oscillation period lengthens (figure not shown).

The second equilibrium state, (42), is located on the straight line $T_e - 2h_e = 0$ and represents an unstable saddle point in the phase space. It is, therefore, physically trivial. Besides, for typical mean state parameters this steady solution is physically unrealistic.

Ⅴ. Nonlinear oscillation

1. *The limit cycle solution*

For the ENSO system, we are more interested in finding out possible finite-amplitude, periodic solution (or limit cycle). If the basic state is time-independent, the ENSO system is a second order autonomous system with one focus and one saddle point. There is at most one limit cycle solution. Furthermore, if a limit cycle exists, it must encircle only the focus point (the equilibrium basic state).

The limit cycle solution occurs in a rather restricted range of the coupling parameter α as shown by the dark shading area in Figure 1b. This domain was determined by numerical integration of (36) and (37). It is a small area imbedded in a much larger domain of linear oscillation. This explains why the search for oscillation in coupled numerical models is often a challenge task.

As expected, the limit cycle is an elliptic encircling the climatological equilibrium state (Figure 2a). The second equilibrium state, being a saddle point, is necessarily located outside the limit cycle. Numerical experiments further demonstrate that the limit cycle is a stable attractor. Any perturbed initial state starting from inside the limit cycle or from outside but within a realistic distance (restricted by the location of the unstable saddle point) will eventually be attracted to the limit cycle.

In physical space, the limit cycle solution represents a perpetual finite-amplitude oscillation as shown in Figure 2b. The thermocline displacement slightly leads SST variation. The decay of warming is faster than the development.

2. *The relevance of the model nonlinear oscillation to ENSO cycle*

Figure 3a shows an observed SST-h scattering diagram for the period of July 1982 to November 1986, roughly one cycle. Each closed circle represents monthly mean anomalies reconstructed from the first two empirical orthogonal functions derived from assimilated ocean data set made by National Center for EnvironmentalPrediction (NCEP) (Ji et al., 1995). Evidently, the limit cycle orbit (Figure 2a) matches observed phase loop in

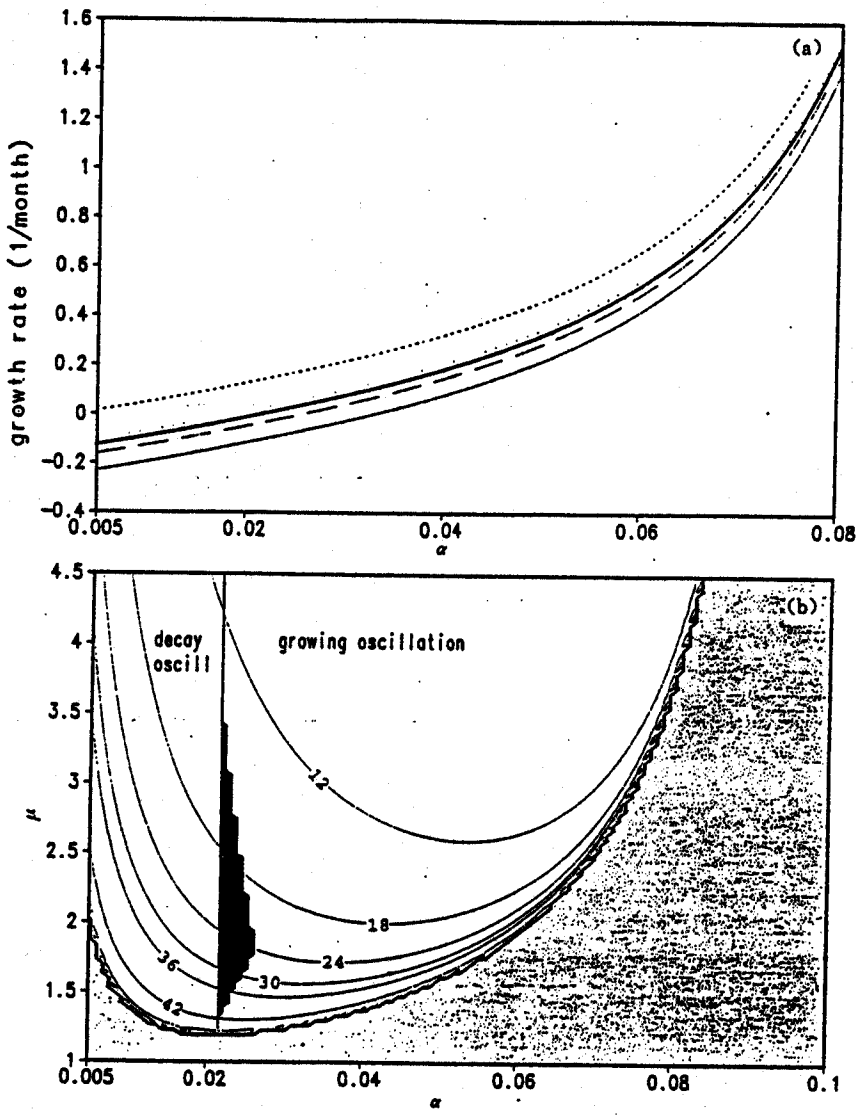

Figure 1 (a) The dependence of growth rate (month^{-1}) on air-sea coupling coefficient α for the basic states of climatological annual mean (thick solid line), January (long dashed line), April (short dashed line), July (dotted line), and October (thin solid line). (b) Period of linear oscillation as functions of α and μ for annual mean basic state. The contour interval is 6 months. Light shading represents the non-oscillatory domain. Dark shading outlines the domain of nonlinear oscillation (limit cycle). The straight line $\alpha = 0.018$ divides the growing and decaying oscillation regime.

anomalous SST-thermocline depth plane (Figure 3a) qualitatively well, suggesting that the model captures basic oscillatory nature of the observed ENSO cycle.

The temporal structure of the model oscillation in SST and h, also bear similarities with the observation. First, the phase of anomalous thermocline depth leads that of SST anomaly by a small fractional cycle in both the model (Figure 2b) and observation (Figure 3b).

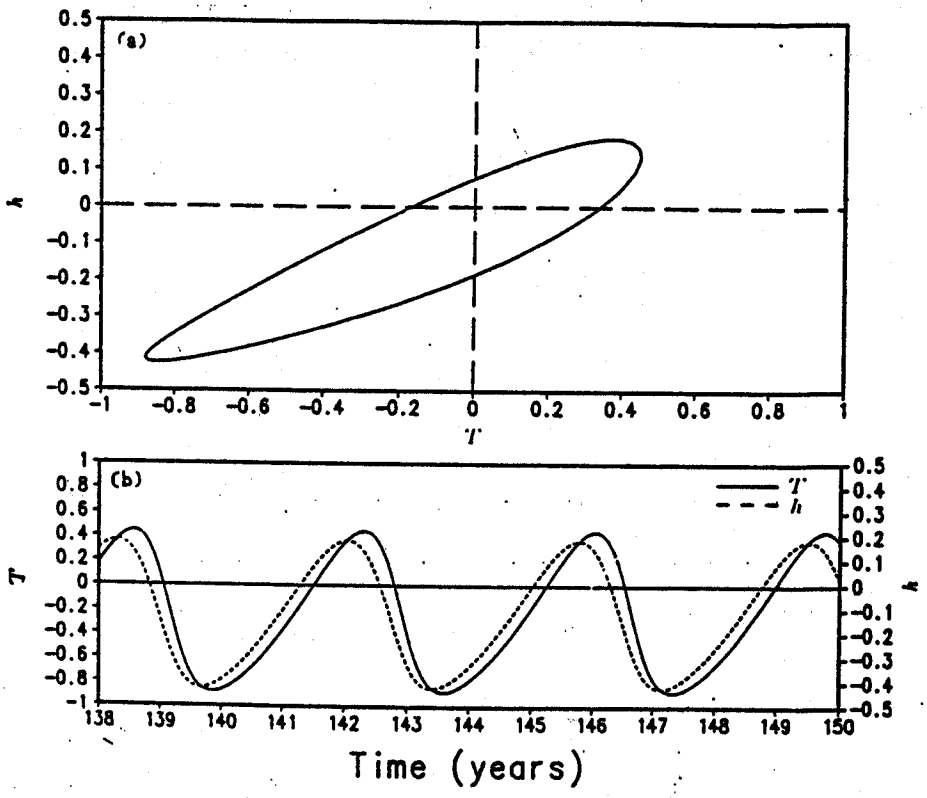

Figure 2 (a) The limit cycle orbit shown in the phase plane. When $\alpha > \alpha_s$ the perturbation initially located near the origin, which represents an climatological mean state, grows and oscillates, approaching the limit cycle. (b) Time series of anomalous temperature (solid line) and thermocline depth (dashed line) from model integration year 138 to year 150. The basic state is annual mean, and $\mu = 1.28$, $\alpha = 0.0192$.

Second, the rise of SST takes longer time than the ensuing collapse (Figures 2b and 3b). The interannual oscillation that appeared in the coupled GCMs of Philander et al. (1992) exhibits the same features.

The aforementioned favorable comparisons add confidence to the relevance of the limit cycle solution to ENSO cycle and to the interannual oscillation found in the coupled numerical models.

3. *Oscillation period and amplitude*

The period and amplitude of the model's nonlinear oscillation depend on climatological mean state and the coupling coefficients. Figure 4a displays the period as a function of coefficients μ and α for the given annual mean state. The oscillation period ranges from 18 months to 60 months. Note that, the period calculated for linear oscillation (Figure 1b), in fact, provides a good estimate for the nonlinear oscillation (Figure 4b). Note also that the oscillation period is primarily determined by the parameter μ. This suggests the importance of the thermocline fluctuation in setting up the time scale for the oscillation.

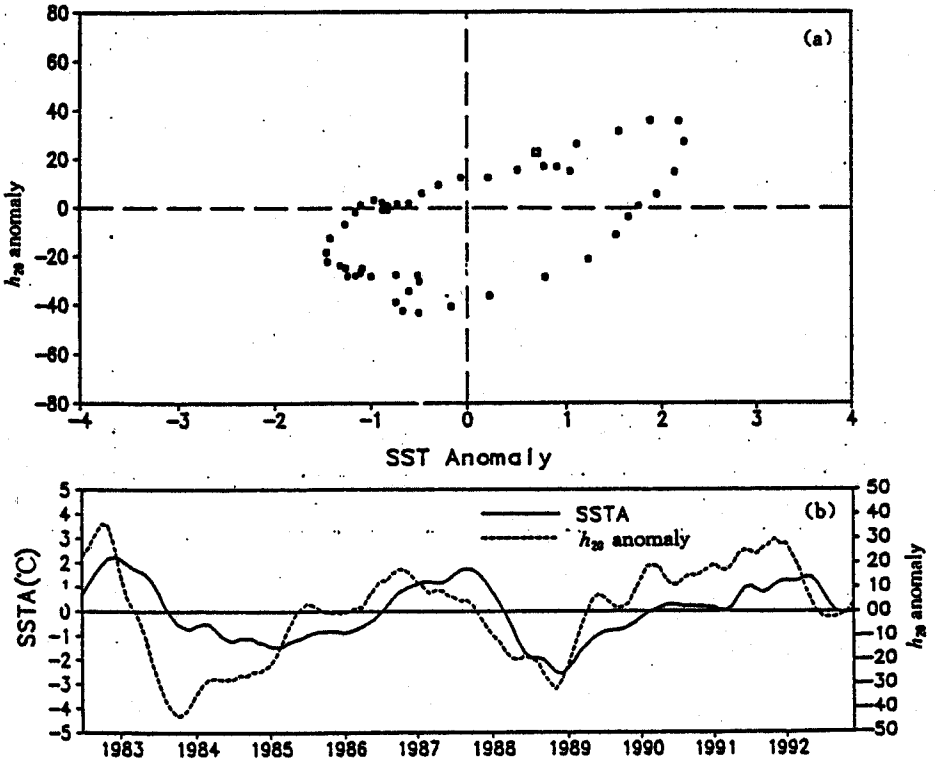

Figure 3 (a) Scattering diagram of observed anomalous monthly mean SST (℃) and depth of 20℃ isotherm (m) averaged over 153°—135°W, 2°S—2°N for the period of July 1982 to December 1986, roughly one cycle. Each closed dot denotes one calendar month. The square denotes the beginning month. (b) Reconstructed anomalous SST and depth of 20℃ isotherm averaged over 153°—135°W, 2°S—2°N for the period from July 1982 to December 1992. Only the first two EOF modes are used for reconstruction. The original data are derived from NCEP ocean reanalysis (Ji et al., 1995).

The amplitude of nonlinear oscillation in SST and thermocline depth are also in a realistic range for the given annual mean basic state (Figures 5a and b). The amplitude increases with increasing μ and α in a comparable rate.

4. *The mechanism of the nonlinear oscillation*

It can be shown that the existence of growing oscillation or limit cycle requires $b > 0$ and $\mu > 2$. To focus on essential mechanisms for the nonlinear oscillation, we assume that $\Delta T'_0 - \alpha'_s = 0$. Equations (36) and (37) reduce to

$$\frac{dT_E}{dt} = -w(T_E)(T_E - \mu h_E), \tag{46}$$

$$\frac{dh_E}{dt} = -b(T_E - 2h_E), \tag{47}$$

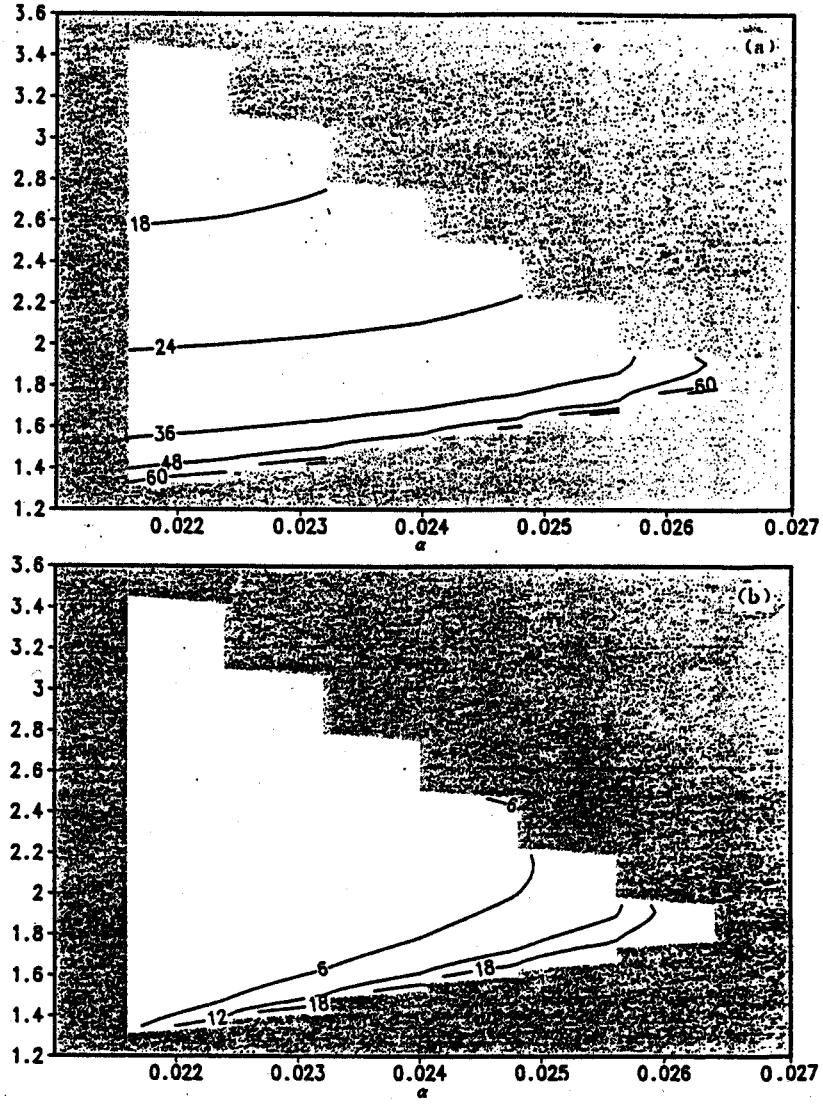

Figure 4 (a) Period of limit cycle as function of α and μ for the annual mean state and (b) period of limit cycle minus period of linear oscillation. The contour interval is 6 months.

where

$$w(T_E) = -(T'_s + \sqrt{\frac{2}{3}}T_E). \tag{48}$$

Figure 6 illustrates how the coupled nonlinear system (46) and (47) oscillates. The two characteristic straight lines $T = 2h$ and $T = \mu h$ partition the limit cycle to four phases. For simplicity, we consider that the total upwelling $w(T) > 0$. During the phase I and II the depending (or shallowing) of thermocline and rising (lowering) of SST take place simultaneously, implying a dominance of the positive feedback between the thermocline displacement and SST. Note, however, that during the phase I and IV, the variation in h and SST have

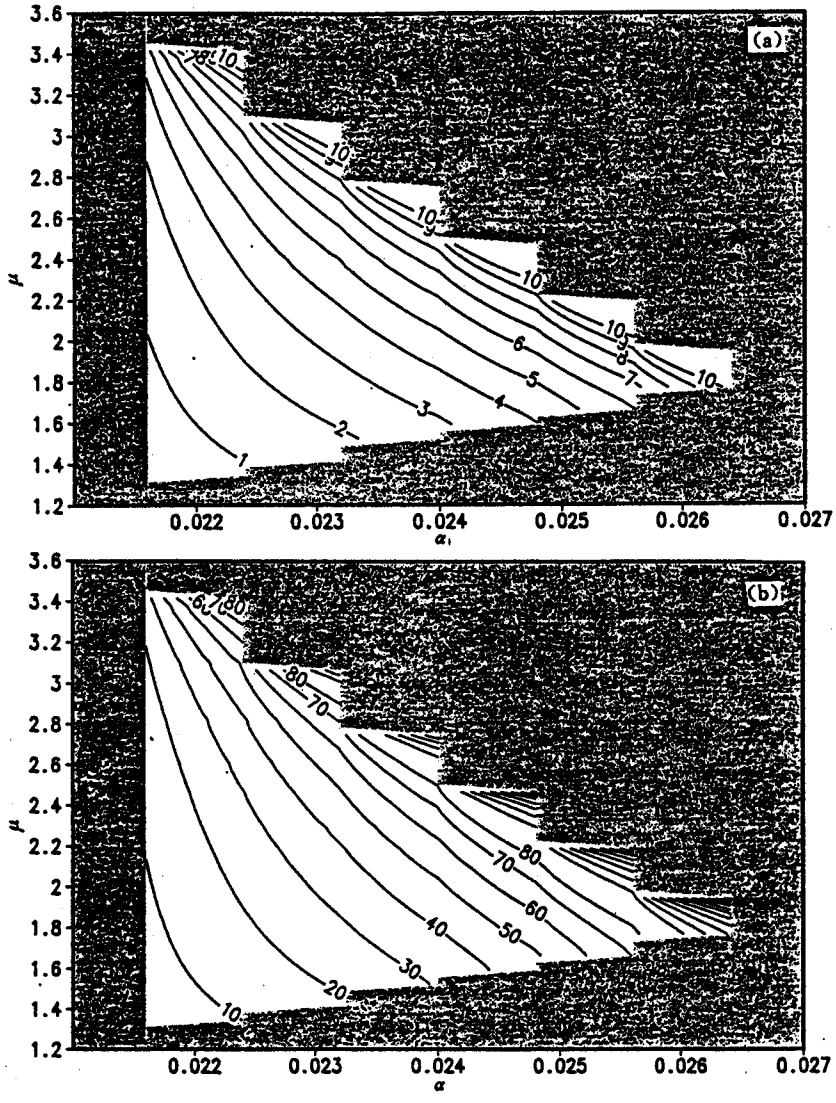

Figure 5 Amplitudes of the limit cycle for (a) SST anomaly (℃), (b) thermocline depth anomaly (m).

in opposite tendency, i. e., increase of SST causes shoaling of thermocline (on phase Ⅰ) or vice versa (on phase Ⅳ). This results in a phase lead of the thermocline displacement to SST variation and provides an negative feedback that turns the coupled system from warming to cooling or vice versa.

The nonlinear h -SST interaction includes a direct influence of h on SST via changing the upwelled water temperature and an indirect feedback from SST to h via changing surface wind. How does thermocline displacement respond to wind or SST variations? In the delayed oscillator model, long equatorial Kelvin and Rossby waves are essential players. In contrast, the slow-SST model (Neelin 1991) denies the roles of these waves and expresses upper ocean dynamics by a diagnostic relation—the Sverdrup balance. To address the above question and

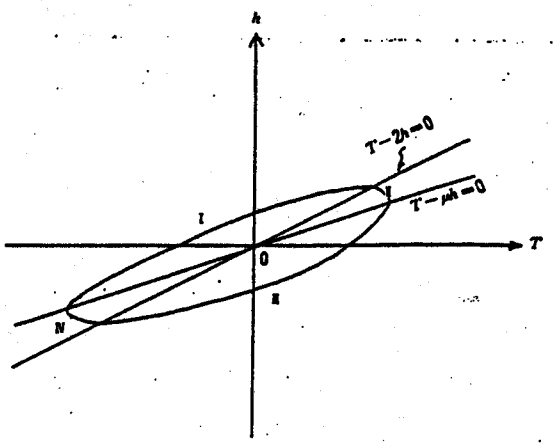

Figure 6 Schematic diagram showing the mechanism of the nonlinear oscillation.

to clarify the roles of various upper ocean dynamic processes, we examine Equation (24) which governs wind forced motion of the upper ocean.

The Sverdrup balance precludes acceleration of zonal currents and Coriolis effect, thereby leads to a degenerated dynamic regime: The evolution of the thermocline field itself can not be determined. To predict slow thermocline variation, which is essential for ENSO, it is imperative to consider a non-Sverdrup balance regime. In fact, the scale analysis in Section Ⅱ indicates that on the ENSO development time scale the ENSO dynamics are essentially of non-Sverdrup balance.

The imbalance between zonal wind stress and pressure gradient force associated with thermocline tilt may bring on two forms of motion: equatorial waves and forced divergent flow. The relative contribution of the two components is measured by parameter ϵ (Equation (27)). In the limit of $\epsilon = 0$, no oceanic wave motion is possible but there remains slow divergent motion forced by wind stress and deflected by Coriolis force. The latter can result in a slow thermocline adjustment. In a coupled system this forced slow motion must be associated with the coupled ENSO mode because the wind is a response to SST. It is important to realize that the wave adjustment is not the only mean for thermocline adjustment. In fact, assuming $\epsilon = 0$ does not upset model's nonlinear oscillation. On the other hand, the slow divergent motion associated with the coupled mode may play a more profound role in the interannual variation of the thermocline.

Ⅵ. Causes of the chaos and season-dependence

With a time-independent basic state, the ENSO system (36) and (37) can have only regular nonlinear oscillation: Chaos does not exist in a second-order autonomous system. When the basic state includes annual cycle, however, the ENSO system becomes non-autonomous, thereby possibly enters a chaotic regime when the amplitude of the basic state annual cycle exceeds a threshold value. This is indeed the case when a reasonably realistic annual cycle is introduced into the basic state. The annual cycle used was obtained by

running a full intermediate tropical Pacific model (Wang et al., 1995) using observed solar radiation, surface wind stress, and cloudiness forcing.

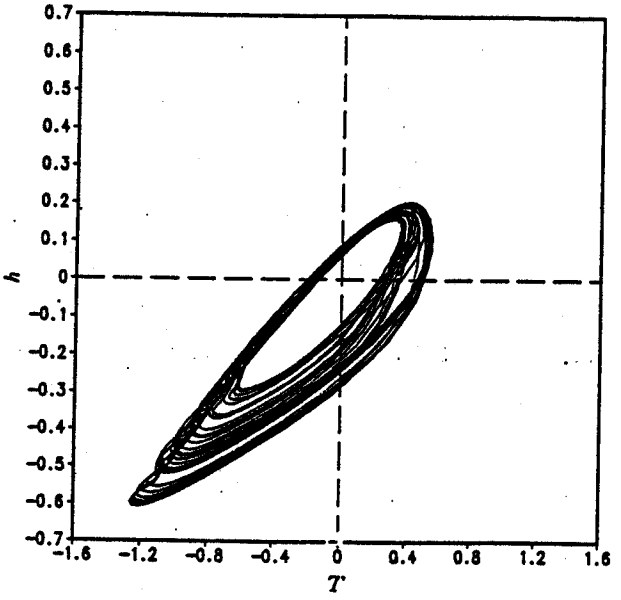

Figure 7 Phase portraits of the strange attractor that represents a chaotic oscillation. Parameters are the same as those in Figure 2 except that an annual cycle basic state is used.

Figure 7 shows phase plane orbits for the chaotic oscillations. The parameters used in the chaotic case are identical to those in the limit cycle case (Figure 2a). The chaotic phase orbits never repeats itself but are trapped to the surroundings of the limit cycle, indicating that the limit cycle is a strange attractor.

The power spectra for regular and chaotic oscillations are compared in Figure 8. For the regular oscillation, a primary energy peak appears on an oscillation period of about 46 months; the secondly subharmonic peaks result from asymmetric temporal evolution of the nonlinear oscillation. The existence of chaos broadens and cuts down the primary energy peak, smears and shifts the subharmonic peaks toward lower frequencies. It is interesting to notice the sharp peak on the annual time scale which manifests the influence of the annual variation of the basic state on the ENSO mode. This resonant response also means a possible rectification of the chaotic ENSO oscillation to the annual cycle of the basic state.

Apparently, the irregularity of ENSO can be caused by other processes. For instance, if the atmospheric high-frequency variations are included in the model, the minimal model would be a third order dynamic system which, even without the annual variation of the basic state, could have chaotic oscillation.

In the eastern tropical Pacific, most El Nino episodes tend to start during the warm phase of the year. Philander (1990) argued that the initiation of unstable ocean-atmosphere interactions requires that unusually warm surface waters cause a local heating of the atmosphere. He speculated that the coupled system is more unstable in boreal spring than

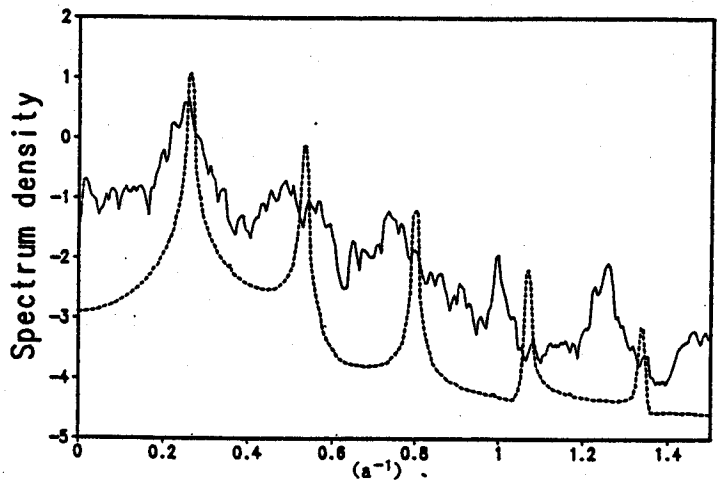

Figure 8 Log spectrum density of anomalous SST for the limit cycle (dashed) and chaotic oscillation (solid) shown in Figures 2a and 7, respectively.

boreal autumn. On the other hand, the numerical results of Battisti and Hirst (1989) implied almost the opposite.

Figure 1a shows that the climatological basic state is most unstable (stable) in boreal spring (fall), confirming Philander's conjecture. For the nonlinear oscillation, perturbation would grow in boreal spring and decay in boreal fall and winter. This means that the weakest east-west thermal contrast (as well as the weakest easterly wind stress and equatorial upwelling) during boreal spring is most unstable to coupled perturbations. Conversely, the cold season tends to reduce coupled instability or resists unstable growth. The ramification is that boreal spring might be the season when the coupled system has weakest persistence or least predictability due to potential fast growth of random perturbations, whereas the boreal fall and subsequent winter basic state possibly levels off the ongoing growth and favors for a mature of warming or cooling.

VI. Summary

With a number of assumptions (none of them distorts the coupled physics in a fundamental way), we derived a simple system of governing equations for ENSO. The system consists of only two equations, one describes oceanic mixed-layer thermodynamics and the other depicts upper ocean dynamics. The atmosphere serves as a medium through which SST anomalies affects thermocline displacement and upwelling. We have shown that the temporal structure of ENSO can be qualitatively described by a second order nonlinear dynamic system.

When the basic state is time-independent (climatological mean for example), the ENSO system is an autonomous system. Beyond a critical value of α the system exhibits a Hopf bifurcation and possesses a unique limit cycle solution that represents a regular, finite-

amplitude oscillation. The limit cycle exists only in a rather restricted domain of α. It is a stable attractor. Any initial perturbation inside the limit cycle or outside the limit cycle (restricted by the location of the second equilibrium state—an unstable saddle point) will eventually be attracted to the limit cycle.

The stable limit cycle describes intrinsic oscillatory behavior of the coupled system. The oscillation is characterized by a lead of thermocline displacement to SST variation and by a temporal asymmetry in its evolution. We have shown that these features resemble some of observed individual ENSO cycles in the 1980s as well as the interannual variations simulated by coupled Ocean-Atmosphere GCMs (e.g., Philander et al., 1992).

The model oscillation is caused by the nonlinear interaction between the thermocline displacement and SST variation. The former affects SST by changing the temperature of the water upwelled into the mixed layer, whereas the SST alters thermocline via changing wind stress and thus the divergence of the ocean currents. This nonlinear interaction involves both a positive and a negative feedback. The latter is characterized by a lead of thermocline fluctuation to SST variation and is responsible for the switch from a warming (or cooling) to an opposing phase.

When the basic state includes annual variations, the ENSO system becomes non-autonomous. The corresponding limit cycle may evolve into a strange attractor. The corresponding oscillation exhibits deterministic chaos. This reveals that the solar radiation forcing may generate ENSO irregularities through controlling the annual cycle of the basic state on which ENSO evolves. Other processes, such as interdecadal variation in the basic state (Wang, 1995), the transients in the atmosphere and ocean, or spatial variability, can also conceivably raise the order of the ENSO system or increase the system's degree of freedom, and generate chaos.

The observed primary peak in the power spectrum of Nino-3 SST anomalies is determined by the period of the limit cycle which, in turn, depends on the basic climatic state, the geometric, rotational, gravitational, and dissipative properties of the coupled system, as well as the coupling coefficients. The dominant period of oscillation does not specifically related to the wave propagation time scales. Note that the subharmonic peaks in the power spectrum may be a result of the asymmetry in the temporal evolution of the nonlinear oscillation. An asymmetric 4—5 year oscillation can induce a sizable quasi-biennial peak. The broadness of the spectral peaks can be simply a manifest of the strange attraction of the limit cycle in the presence of basic-state annual cycle.

The model, however, is far from realistic and by no means perfect. We have kept the model as simple as possible for the purpose of qualitatively understanding the basic mechanisms of the Southern Oscillation. Many modifications or extensions can be made to implement and improve the model's physics and mathematical representations.

One of the major limitations that arises from the crucial truncation in longitudinal direction is that the present model is unable to explain the eastward propagation of the upper ocean heat content associated with ENSO. This feature was simulated by OGCM (Chao and

Philander, 1993) and confirmed by our recent analysis of the NMC assimilated data; the eastward propagation of thermocline depth is prominent in the equatorial western-central Pacific. This underlines a need for future studies.

Acknowledgments I have the honor to contribute this paper to the Eightieth Birthday Volume in honor of Professor Ye Duzheng's life-time, outstanding contributions to Atmospheric Sciences. I would like to take this opportunity to express my sincere gratitude for Prof. Ye's long-standing guidance and encouragement not only for me but the entire young generations of the Chinese meteorologists. Thanks are also extended to Mr. Zheng Fang who carried out all numerical computations and prepared seven figures, to Mr. Renguang Wu for drawing Figure 3., and to Mr. Yan Wang for preparing the manuscript. This study is supported by NOAA GOALS and PACS programs under a cooperated agreement. The views expressed herein are those of the author and do not necessarily reflect the view of NOAA or any of its sub-agencies. This is the School of Ocean and Earth Science and Technology publication number XXXX.

Appendix *Derivation of Free Wave Solutions*

In the absence of wind forcing, the nondimensional thermocline-depth equation becomes

$$\frac{\partial}{\partial t}\left[y^2 h + \left(\frac{2}{y} - \frac{\partial h}{\partial y} - \frac{\partial^2 h}{\partial y^2}\right)\right] - \frac{\partial h}{\partial x} = 0, \tag{A.1}$$

where y and t are scaled by $(g'H)^{1/4}\beta^{-1/2}$ and $(g'H)^{-1/4}\beta^{-1/2}$, respectively. Assume

$$h(x, y, t) = \mathrm{Re}[y \cdot H(y)e^{ik(x-ct)}]. \tag{A.2}$$

The amplitude function $H(y)$ is bounded as $|y| \to \infty$ and satisfies, from (A.1),

$$\frac{d^2H}{dy^2} - \left(\frac{1}{c} + y^2 + \frac{2}{y^2}\right)H = 0. \tag{A.3}$$

Equation (A.3) has eigen solution of the following from (Hochstrasser, 1965)

$$H_n(y) = e^{-y^2/2}y^{\alpha+\frac{1}{2}}L_n^{(\alpha)}(y^2), \tag{A.4}$$

where $L_n^{(\alpha)}(x)$ denotes generalized Laguerre function

$$L_n^{(\alpha)}(x) = \sum_{k=0}^{n}(-1)^k\binom{n+\alpha}{n-\alpha}\frac{x^k}{k!}, \tag{A.4a}$$

with

$$\alpha = \pm\frac{3}{2}, \tag{A.5}$$

and

$$c = \begin{cases} -\dfrac{1}{4n+5} & \left(\alpha = \dfrac{3}{2}\right), \\ -\dfrac{1}{4n-1} & \left(\alpha = -\dfrac{3}{2}\right), \end{cases} \quad n = 0, 1, 2, \cdots \tag{A.6}$$

The mode with $\alpha = -3/2$ and $n = 0$ is the Kelvin wave whose phase speed $c = 1$ and meridional structure is $e^{-y^2/2}$. The modes with $\alpha = -3/2$ and $n = 1, 2, \cdots$ are symmetric long Rossby waves whose phase speed

$$c = -\frac{1}{3}, -\frac{1}{7}, -\frac{1}{11}, \cdots \tag{A.7a}$$

and meridional structures are

$$e^{-y^2/2} L_n^{(-3/2)}(y^2). \tag{A.7b}$$

The modes with $\alpha = 3/2$ and $n = 0, 1, 2, \cdots$ are antisymmetric long Rossby waves whose phase speed

$$c = -\frac{1}{5}, -\frac{1}{9}, -\frac{1}{13}, \cdots \tag{A.8a}$$

and meridional structures are

$$e^{y^2/2} y^3 L_n^{(\frac{3}{2})}(y^2). \tag{A.8b}$$

References

Battisti, D. S., and A. C. Hirst, 1989: Interannual variability in the tropical atmosphere-ocean system: Influence of the basic state and ocean geometry, *J. Atmos. Sci.*, **46**, 1678.

Bjerknes, J., 1966: A possible response of the atmospheric Hadley circulation to equatorial anomalies of ocean temperature, *Tellus*, **18**, 820—829.

Bjerknes, J., 1969: Atmospheric teleconnections from the equatorial Pacific, *Mon. Wea. Rev.*, **97**, 163—172.

Cane, M. A., 1979: The response of an equatorial ocean to simple wind stress pattern I. Model formulation and analytical results, *J. Mar. Res.*, **37**, 233—252.

Cane, M. A., M. Munnich and S. E. Zebiak, 1990: A study of self-excited oscillations of the tropical ocean-atmosphere system, Part I: linear analysis, *J. Atmos. Sci.*, **47**, 233—252.

Chao, Y., and S. G. H. Philander, 1993: On the structure of the Southern Oscillation, *J. Clim.*, **6**, 450—469.

Gill, A. E., 1980: Some simple solutions for heat-induced tropical circulation, *Quart. J. Roy. Meteor. Soc.*, **106**, 447—462.

Gu, D., and S. G. H. Philander, 1995: Secular changes of annual and interannual variability in the tropics during the past century, *J. Clim.*, **8**, 864—876.

Hochstrasser, U. W., 1965: Orthogonal polynomials, *Handbook of Mathematical Functions*, M. Abramowitz and I. A. Stegun, Eds., Dover Publications, New York, pp 1046.

Ji, M., A. Leetmaa and J. Derber, 1995: An ocean analysis system for seasonal to interannual climate studies, *Mon. Wea. Rev.*, **123**, 460—481.

Kessler, W. S., 1990: Can reflected extra-equatorial Rossby waves drive ENSO, *J. Phys. Oceanogr.*, **21**, 444—452.

Latif, M., A. Sterl, E. Maier-Reimer and M. M. Junge, 1993: Structure and predictability of the El Nino/Southern Oscillation phenomenon in a coupled ocean-atmosphere general circulation model, *J. Clim.*, **6**, 700—708.

Lindzen, R. S., and S. Nigam, 1987: On the role of sea surface temperature gradients in forcing low level winds and convergence in the tropics, *J. Atmos. Sci.*, **44**, 2418—2436.

Matsuno, T., 1966: Quasi-geostrophic motions in the equatorial area, *J. Meteor. Soc. Japan*, Ser. I **44**, 25—43.

McCreary, J. P., and D. L. T. Anderson, 1991: An overview of coupled ocean-atmosphere models of El

Nino and the Southern Oscillation, *J. Geophys. Res.*, 96, 3125—3150.

Neelin, J. D., 1991: The slow sea surface temperature mode and the fast-wave limit: analytic theory for tropical interannual oscillations and experiments in a hybrid coupled model, *J. Atmos. Sci.*, 48, 584—606.

Neelin, J. D., M. Latif and F.-F. Jin, 1994: Dynamics of coupled ocean-atmosphere models: The tropical problem, *Annu. Rev. Fluid Mech.*, 26, 617—695.

Philander, S. G. H., 1990: *El Nino, La Nina and the Southern Oscillation*, Academic Press, 293 pp.

Philander, S. G. H., T. Yamagata and R. C. Pacanowski, 1984: Unstable air-sea interaction in the tropics, *J. Atmos. Sci.*, 41, 604—613.

Philander, S. G. H., R. C. Pacanowski, N. C. Lau and M. J. Nath, 1992: Simulation of ENSO with a global atmospheric GCM coupled to a high-resolution, tropical Pacific ocean GCM, *J. Clim.*, 5, 308—329.

Rasmusson, E. M., and T. H. Carpenter, 1982: Variations in tropical sea surface temperature and surface wind fields associated with the Southern Oscillation/El Nino, *Mon. Wea. Rev.*, 110, 354—384.

Saurez, M. J., and P. S. Schopf, 1989: A delayed action oscillator for ENSO, *J. Atmos. Sci.*, 45, 3283—3287.

Schopf, P. S., and M. J. Suarez, 1990: Ocean wave dynamics and the time scale of ENSO, *J. Phys. Oceanogr.*, 20, 629—645.

Sverdrup, H. U., 1947: Wind-driven currents in a baroclinic ocean with application to the equatorial currents of the eastern Pacific, *Proceedings of the National Academy of Sciences*, 33, 318—326.

Wang, B., 1995: Interdecadal changes in El Nino onset in the last four decades, *J. Clim.*, 8, 267.

Wang, B., and T. Li, 1993: A simple tropical atmosphere model of relevance to short-term climate variations, *J. Atmos. Sci.*, 50, 260—284.

Wang, B., T. Li and P. Chang, 1995: An intermediate model of the tropical Pacific ocean, *J. Phys. Oceanogr.*, in press.

Wang, B., Y. Wang, 1995 Temporal structure of the Southern Oscillation as revealed by waveform and wavelet analysis., submitted to *J. Clim.*

Wang, C., and R. H. Weisberg, 1994: On the "slow mode" mechanism in ENSO-related coupled ocean-atmosphere models., *J. Clim.*, 7, 1657—1667.

Zebiak, S. E., and M. A. Cane, 1987: A model El Nino-Southern Oscillation, *Mon. Wea. Rev.*, 115, 2262—2278.